International Journal of Advanced Technology and Engineering Exploration, Vol 10(99)
ISSN (Print): 2394-5443 ISSN (Online): 2394-7454
http://dx.doi.org/10.19101/IJATEE.2021.876104

Research Article

Transmission line fault analysis using ANN and Rogowski coil

A. N. Sarwade[1*], M. M. Jadhav[2] and Shivprasad P. Patil[3]
Professor, Department of Electrical Engineering, Sinhgad College of Engineering, Pune, Maharashtra, India[1]
Professor, Department of Electronics and Telecommunication, NBN Sinhgad Technical Institutes Campus, Pune, Maharashtra, India[2]
Professor, Department of Information Technology, NBN Sinhgad Technical Institutes Campus, Pune, Maharashtra, India[3]

Received: 03-June-2022; Revised: 20-February-2023; Accepted: 24-February-2023

Abstract
High voltage transmission lines (HVTL) are susceptible to numerous faults. In fact, the percentage of faults occurring on a transmission line (TL) is typically in the range of 80-85% when compared to total faults in the entire power system. If a prompt and efficient countermeasure is not adopted once a fault occurs, it may propagate to other equipment and, in the worst-case scenario, lead to a system-wide blackout. Therefore, fault diagnosis in HVTLs remains a challenging problem, and there is a need for a reliable and efficient transmission line distance protection scheme, as well as an exceptional fault diagnosis method to handle this challenging task. In this paper, a viable fault diagnosis approach using artificial neural networks (ANN) is proposed to achieve an efficient, reliable, and secure TL distance protection scheme. The Rogowski coil is utilized as an alternative to conventional current transformers due to its built-in linear working characteristics. Ten different fault types are created on a typical 200 km, 220 kV TL, each with different fault inception angles and resistances at five various locations, for experimentation purposes. A conventional tool is used to generate the data set containing the apparent impedance values necessary for the proposed model. The presented method establishes a good relationship between apparent impedances, fault types, and fault locations. Finally, the results show that the proposed model is more accurate than existing approaches.

Keywords
Artificial neural network, Current transformer, Distance protection scheme, High voltage transmission lines.

1.Introduction
Electrical energy is generated, transmitted, and delivered to various types of customers at the appropriate voltage and frequency through an electrical network consisting of generators, transmission lines (TL), distribution lines, and transformers, all of which perform incredibly well [1]. Both industry and educational sectors are increasingly adopting hybrid modes of working environments in their daily operations. Additionally, modern citizens are demanding an ever-increasing level of security and reliability in their electric supply. Therefore, considering frequent and prolonged power failures due to environmental conditions, calamities, human errors, tree falls, and equipment malfunctions, a well-planned and designed electric network is necessary to avoid interruptions to scheduled activities. As a result, an electric network needs to be built to provide affordable and consistent electrical energy [2].

Corrected statement: High voltage transmission lines (HVTL) are the most cost-effective and efficient method for transporting large amounts of energy over long distances. However, it has been observed that the number of faults occurring on TL is higher compared to the overall faults in the entire electric power grid. If corrective action is not taken after a fault, it may spread to other equipment, leading to a system-wide blackout in extreme cases. Therefore, adequate protection must be provided for the TL network to quickly identify and resolve various abnormal conditions, preventing power loss or cascade tripping of the electric power grid [3]. Over-current and distance protection (DP) techniques are exclusively used to protect HVTL. DP is the most significant and well-known relaying method used to protect HVTL and sub-TL from electrical fault conditions [4].

To accelerate the system restoration process after a fault in DP, it is essential to quickly evaluate the type

*Author for correspondence

and location of the fault. Conventional fault-finding methods, such as patrolling, may be time-consuming, especially in the case of long-distance TLs, prolonging the fault repair process. On the other hand, the reliability of a fault diagnosis technique depends on the quality of data collected and processed, including previous fault finding and classification records [5]. This creates the motivation to develop a more reliable DP scheme and explore more specialized fault diagnosis methods for HVTL.

The prime objective of the fault diagnosis method is twofold [6]:
Fault classification: The ability to classify the type of fault and the affected phase/phases.
Fault location: The ability to locate the fault point in terms of distance on the transmission line.

To minimize damage and disruption to the power system, an artificial neural network (ANN)-based DP scheme is proposed in this paper. It is developed to accurately detect and isolate various kinds of disturbances. Ten types of faults are created on HVTL at different fault distances (FD) with various fault inception angles (FIA) and fault resistances (RF). The Rogowski coil (RC) is used instead of a conventional current transformer (CT) to measure the current and feed it to the distance relay (DR). In this work, the apparent impedance (Zap) values are estimated under several fault scenarios using the current and voltage signals from the RC and the voltage transformer (VT), respectively. The estimated Zap values are used to create the dataset required to train and test the ANN model. It is observed that the trained ANN model can accurately determine the fault types and distances on the HVTL. The simulation is performed using the Power System Computer Aided Design-Electromagnetic Transient DC (PSCAD-EMTDC) 4.1 software.

The paper is organized into six sections. A literature review on the adoption of RC and other fault diagnosis techniques is presented in section 2. Whereas, section 3 discusses the significance of RC and ANN for the classification and location of faults. Section 4 presents the analysis of the results, whereas the discussion of the results is elaborated in Section 5. Finally, the conclusions and scope for future work in this area are discussed in section 6.

2.Literature review

Literature review has been carried out in two parts. Parts one gives details of the adoption of the RC in place of conventional CT and part two about selection of fault diagnosis method.
Part 1: In distance protection scheme (DPS), the performance of CTs & VTs is of the utmost importance, as the lowered secondary values must be an exact replica of the primary side values under all normal & abnormal scenarios [7]. Under abnormal conditions, more transients are present in primary line currents than line voltages. Presence of transients in current leads to CT saturation at earlier stage, which subsequently distort the nature of secondary current waveform [8]. Distortion in current waveform changes the value of estimated impedance and causes DR to under reach or over-reach [9, 10]. Thus faithful transformation of current signal on CT secondary side is very important in getting correct trip decision from DR. Hence it is very important to search for the solution on CT saturation problem, which will help to improve performance of DP scheme.

To get rid from CT saturation issue and to improve current measurement method, different techniques, algorithms are addressed to reconstruct distorted waveform. Apart from this some alternatives to conventional CT, like optical current sensors, gapped core CT, linear couplers are suggested by some authors to enrich current measurement. The algorithm recommended in [11], is unaffected by CT saturation-related consequences and gives correct FD. But in this proposed algorithm, currents retrieved from one unsaturated CT is considered as an input signal. The method proposed in [12] claims selectivity reliability, speed for all faults under CT saturation in differential impedance protection scheme. However, deficiency in proposed method in noted in identifying correct fault location. The model based method suggested in [13] used to identify and overcome CT saturation in which tentative values for some variables such as residual flux, winding impedance, inductive burden, and so on are considered. In [14, 15], effective algorithm has been proposed to overcome CT saturation in relaying operation. This approach is more effective, as no additional equipment are required and the configuration of the relaying circuits remaining intact. However, this approach does not fit in all scenarios and there is also a requirement of modern relays with the ability to assist CT saturation correction phenomena.

In [16] it is suggested to increase CT size to prevent CT saturation, which may not accommodate in the previously implied areas as well as may not be economically feasible. In [17], author proposed

utilizing a fiber optic current sensor for current measurement, however it was found to be both expensive and difficult to build accurate measurement systems with it in conventional substations.

With modern multifunction relays, RC facilitate the development of advanced metering, control, and protection schemes, allowing faster fault response time and the ability to easily adapt with change in load and/or power system structure. As, new RCs are so exact, degree of protection can be adjusted to reduced threshold limits, minimizing burden on the protected apparatus. Furthermore, metering and control mechanism work quite correctly. The cost of RC is very less (almost 1/10th times) when compared with cost of conventional CT of same current rating [18]. In addition to this, RC is widely employed in a wide range of applications, like the measurement of power frequency current, the measurement of impulse and pulsed currents [19–21], the measurement of currents in smart meters [22], fault detection mechanisms [23, 24], and many more. The main reasons behind the adoption of RC are its flexibility and simplicity in design. The printed circuit board design is the most recent and widely used design of RC used in numerous applications [25–27].

Part 2: In case of long TL's, fault diagnosis methods requires detailed information about the transients present in current and voltage waveforms after fault. In part 1, several methods have been proposed on recovery/modification/ characteristics extraction of distorted current waveform [11–13]. However, the choice of the suitable extracted characteristics depends on one's proficiency in this area and can be distinct. Using appropriate algorithms the required characteristics present in the waveforms can be extracted [28, 29]. But, these methods increases the computational load as well as the need of expertise or fine-tuning before being applied to new systems. As a result the flexibility and applicability of the proposed methods gets reduced.

Only high frequency coefficients of wavelet transform (WT) have been used for fault identification, classification and location [30]. A very high sampling frequency of 200 kHz used in another WT based technique proposed for fault diagnosis in series compensated lines may prove to be a slightly challenging for practical execution [31]. Analysis on the use of expert systems for fault diagnosis shows that neural networks (NN)s have been found successful due to their generalization capability while dealing with uncertainties related with different types of fault parameters in HVTL's [32–34].

Hence, ANN has been found to be computationally fit and capable of handling massive datasets and offer excellent adaptation capabilities for classification issues.

3.Methods

3.1Fault identification and fault location using ANN

The primary goal of ANN in TL protection is to enhance the DPS's ability to diagnose faults more efficiently and accurately. The use of ANN for fault classification and finding faults on HVTL's is described in detail in this section.

Further, it is observed that improving the stability, security, safety, and reliability of the electrical power system requires quickly identifying the type and location of a fault. It helps to accelerate the process of system restoration after a fault. With the help of data that was collected and processed using records from prior fault detection and its classification, the reliability of a fault diagnosis technique is enhanced in this work. *Figure 1* shows the block diagram for fault analysis on 220 kV, 200 km, 50 Hz three-phase HVTL using ANN and RC. After creating ten FT's with various FD's, FIA's & RF's, current and voltage signals are measured to calculate the value of Zap's. The targeted signature pattern is compared with the actual generated signature pattern to classify a total of 10 faults and identify their locations.

DPS is an established relaying technique used to protect the HVTL and sub-TL against electrical fault conditions (*Figure 2*). According to this scheme, fault analysis is done by estimating Zap up to the fault location using a VT and CT secondary values that are captured at the location of the DR. Further, estimated Zap is compared with the reach point impedance, for fault detection. If the Zap is less than the reach point impedance, a fault exists on the line between the relay and the reach point r [9].

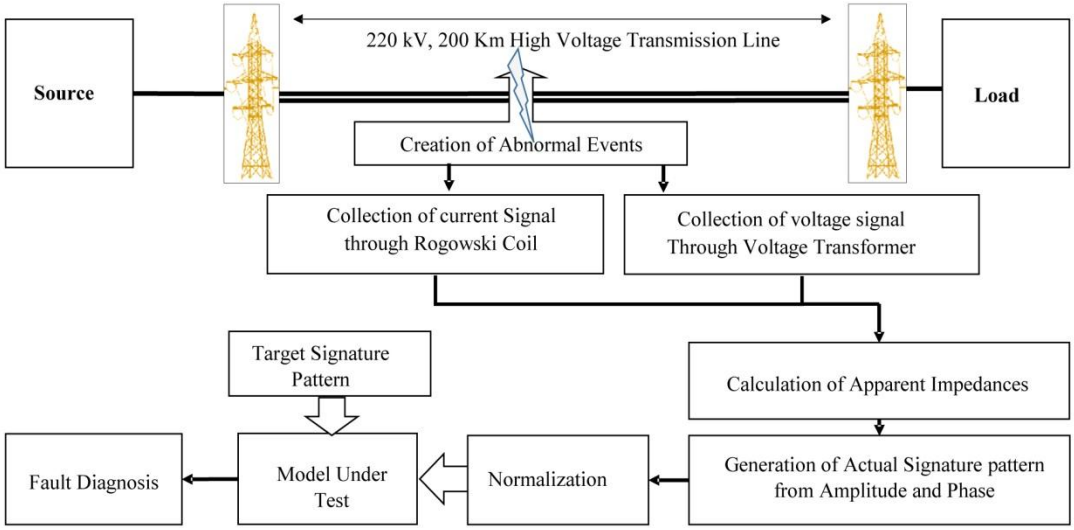

Figure 1 Block diagram for TL fault analysis using ANN and RC

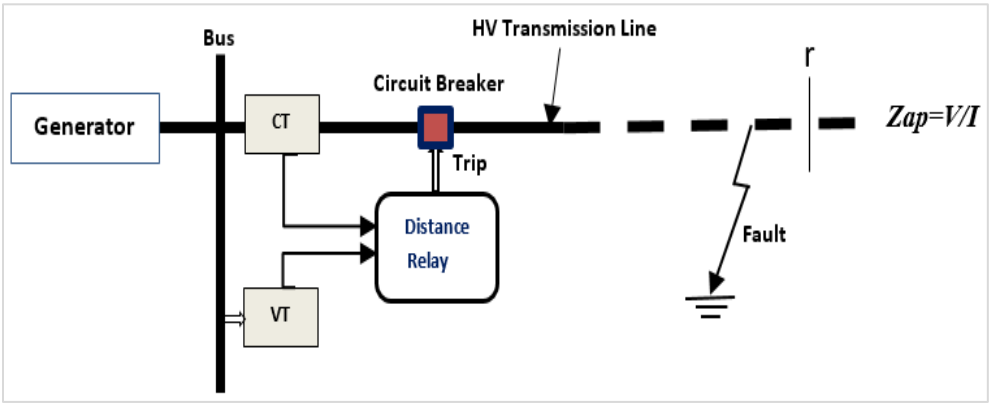

Figure 2 Distance protection scheme

Estimation of Zap: In three phase DPS, three units are used to detect line-to-line faults and another three units are used for earth faults detection [35]. In the case of line-to-line fault, the *Zap's* is the ratio of voltages and currents and is given by Equations 1 to 3 as

$$Z_{AB} = \frac{V_A - V_B}{I_A - I_B} \quad (1)$$

$$Z_{BC} = \frac{V_B - V_C}{I_B - I_C} \quad (2)$$

$$Z_{CA} = \frac{V_C - V_A}{I_C - I_A} \quad (3)$$

In the case of an earth fault, the Zap given by Equations 4 to 6 as

$$Z_A = \frac{V_A}{I_A\left(1+\frac{Z_0 - Z_1}{3Z_1}\right)} \quad (4)$$

$$Z_B = \frac{V_B}{I_B\left(1+\frac{Z_0 - Z_1}{3Z_1}\right)} \quad (5)$$

$$Z_C = \frac{V_C}{I_C\left(1+\frac{Z_0 - Z_1}{3Z_1}\right)} \quad (6)$$

The experimentation set-up for fault identification and location with the ANN technique using RC as a current transducer is illustrated in *Figure 3*. This technique makes use of Zap estimated for different types of faults created at different locations on a transmission line with different R_F's and FIA's. The major components involved in the experimental setup are described below in sections 3.1 and 3.2.

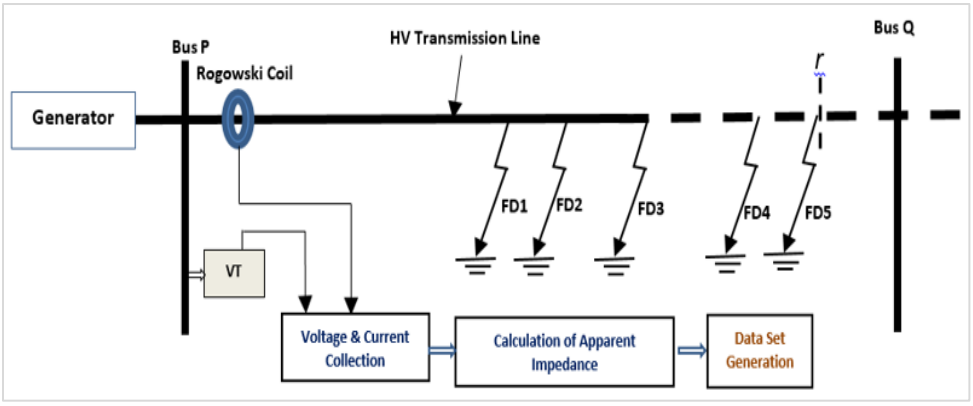

Figure 3 Experimental setup for calculation of apparent impedance

3.1.1Transmission line protection using Rogowski coil

According to the study, correct trip decisions from DR rely on the faithful transformation of the current signal on the secondary side of the CT. RC is a solution for CT saturation that helps to improve the performance of DPS. The fundamental distinction between RC and CT is that RC windings are uniformly wound around nonmagnetic or air core rather than the core made up of magnetic material as shown in *Figure 4*. RC enables the design of modern control, protection and metering schemes with advanced multipurpose relays, providing faster response times to faults and can easily adjust to changes in power system configurations. The mutual inductance must be consistent for any primary conductor position within the coil ring to meet the first criterion. This is feasible by providing a coil with a constant cross-section S over an air/nonmagnetic core and building a coil with a specific turn density n. and Mutual inductance is given by Equation 7 [36, 37].

$$M = \mu_0 \, n \, S \qquad (7)$$

Where μ_0 is the permeability of air / nonmagnetic material. Further, RC output voltage (V_{out}) in terms of the current to be measured is shown by Equation 8.

$$V_{out} = -M \frac{di(t)}{dt} \qquad (8)$$

The input-output characteristics of RC used for experimentation are shown in *Figure 5* [38].

Two source AC power system model: As shown in *Figure 6*, fault analysis in DPS is performed using PSCAD-EMTDC 4.1 on a section of a 220 kV AC system [39]. The details of the 220 kV system used for the case study are given in *Table 1* [40].

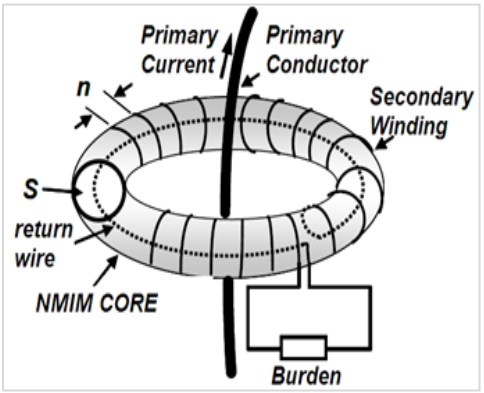

Figure 4 Rogowski Coil (RC) configuration

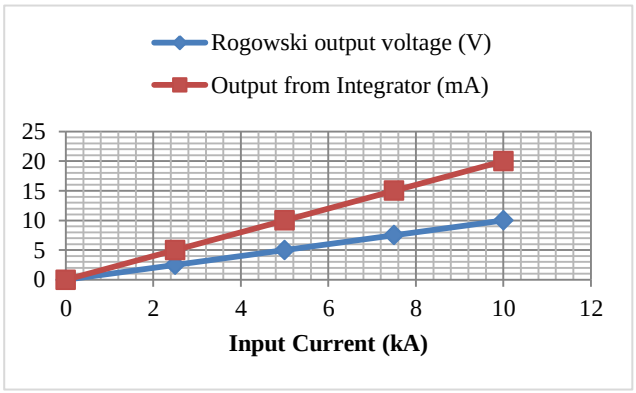

Figure 5 Experimented V-I characteristics

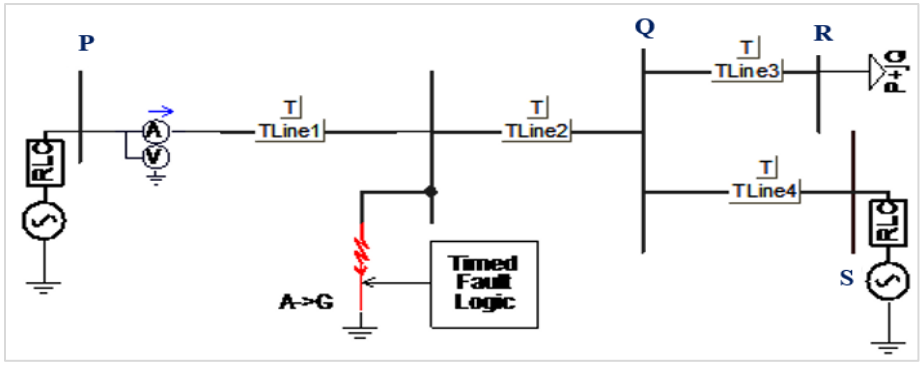

Figure 6 Simulated two source AC power system model

Table 1 220 kV AC system details used for experimentation

S. No.	Term	Ratings
1	System mega volt amps (MVA)	100 MVA
2	+ve sequence impedance (per km), Z_1	$0.2928\angle 86.57^0\ \Omega$
3	0 sequence Impedance (per km), Z_0	$1.11\angle 74.09^0\ \Omega$
4	TL PQ length	200 km
5	Source Impedance	$32.15\angle 85^0\Omega$
6	Source Voltage	220 kV, 50Hz
7	compensation factor	2.82
8	Load	(75+j25) MVA

RC details used in 220 kV AC system: The RC model along with an integrator as shown in *Figure 7* is used in DPS and based on the 220 kV system rating, its parameter values are estimated [40, 41]. The specifications of the RC model are given in *Table 2*.

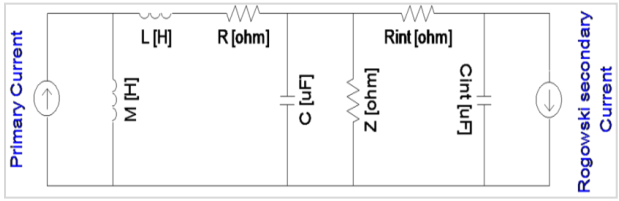

Figure 7 RC model in PSCAD

Table 2 Rogowski coil ratings

S. No.	Term	Ratings
1	Rated Current	100kA
2	RC Output	1000 mV/1 kA
3	RC winding turns	270
4	M of RC	2 µH
5	R, L of RC	186 Ω, 7.8 mH
6	C & Z of RC	235 pF, 2 k Ω
7	Integrator R (R_{int}) & C (C_{int})	100 Ω, 1 µF

3.1.2ANN in transmission line protection

Fault diagnosis using ANN is imperative due to its learning ability. For different fault events created on lines, 560 samples are collected and used to train the network. Further, the gradient descent algorithm is used to find out the error. The application of ANN in TL protection is primarily concerned with developments in attaining more efficient and effective fault diagnosis in DPS. Here, 50 % data is used for training, 25% of data for testing, and 25 % for validation to identify the type and location of the fault. *Table 3* shows the fault events created on the 220 kV system under consideration to observe the consistency of RC under abnormal conditions.

Table 3 Fault events created on a line between bus P and bus Q

S. No.	Power system events	Details	
1	FT	Line to ground (LG)	Phase A to ground (AG) Phase B to ground (BG) Phase C to ground (CG)
		Line to line (LL)	Phase A to phase B (AB) Phase B to phase C (BC)

S. No.	Power system events	Details	
			Phase C to phase A (CA)
		Line to line to ground (LLG)	Phase A to phase B to ground (ABG) Phase B to phase C to ground (BCG) Phase C to phase A to ground (CAG)
		Line to line to line (LLL)	Phase A to phase B to phase C (ABC)
2	FIA	0^0, 30^0, 45^0 and 90^0	
3	FD	10% of line P-Q : 20 km	
		25% of line P-Q: 50 km	
		50% of line P-Q: 100 km	
		75% of line P-Q: 150 km	
		80% of line P-Q: 160 km	
4	R_F	0 Ω and 10 Ω	

Algorithm for fault diagnosis:

The algorithm to identify the FT and FD on the transmission line using the ANN approach is explained below:

Input: TL length: 200 km
Fault distance in km: FD1=20, FD2=50, FD3=100, FD4=150 and FD5= 180.
Fault Inception Angle (FIA): 0^0, 30^0, 45^0 and 90^0
Fault Type (FT): LG, LL, LLG, and LLL
Fault Resistance (R_F): 0 Ohm and 10 Ohm
Voltages and currents at all possible combinations of FT's, FD's, FIA's & R_F's
ANN with: 3 input nodes, hidden neurons variation range: [10, 15, 20, 25, 30, and 35], learning rate: 0.001 and 0.005 & the number of epochs: 300, during the training of ANN.

Output: Estimation of Zap values

Start

Step 1: Initialize 200km, 220 kV AC power system as per *Table 1*.
Step 2: Collect voltage and current values at a specific FD for all ranges of FIA's, FT's, and R_F's.
Step 3: Estimate the values of the Zap seen by each phase as well as between two phases.
Step 4: Create data–Set for all possible combinations as mentioned in step 2.
Step 5: Train the ANN model for FT identification by considering the impedance seen by each phase and fault location by considering the impedance seen across two phases.
Step 6: Test and validate the model for the accuracy of FT and FD.
The network consists of :
a) Set of N input units $\{X_i\}$; where i = 1, 2,…, N
b) Set of n output units$\{Y_k\}$; where k =1, 2,…, n
c) Set of j hidden units $\{V_j\}$; where j = 1, 2,…, j
Thus, the hidden unit receive a net input and produce the output given by equation 9

$$Y_i = F\left[\sum_{m=1}^{j} W_{im} V_m\right] \quad \text{Where i = 1, 2,…, n.} \qquad (9)$$

End

4.Results

A series of simulations have been executed in order to determine the effectiveness of the proposed protective scheme. These simulations are then used to generate the required data for training and testing in this work. The following processes are carried out to obtain the simulation results:-

Process 1: Initialisation of model

- Create faults such as LG, LL, LLG, and LLL for different FIA's, FD's, and R_F's.
- Observe and store the value of Zap, read by phase A, phase B and phase C respectively.
- Thereafter, again create LL and LLL faults for different FIA's, FD's, and R_F's.

- Observe and store the value of Zap involving between phases AB, phases BC and phases CA respectively.

Process 2: Data collection and sault diagnosis results using RC

- Create all ten types of faults at 20 km, 50 km, 100km, 150 km, and 160 km FD's. Adjust FIA to 0^0, 30^0, 45^0, and 90^0 as well as R_F to 0 Ω and 10 Ω.
- Collect 560 samples for training the proposed network.
- Zap values seen across individual phases A, B, and C are used for FT classification. Ten types of faults such as A-G, B-G,…, and A-B-C are assigned as F_0, F_1,…, and F_9.
- Zap values seen across phases A-B, B-C, and C-A are used for finding the FD. FD's, 20 km, 50 km, 100 km, 150 km, and 160 km are assigned as F_{D0}, F_{D1}, F_{D3}, and F_{D4} respectively.
- A binary string of 9 bits is assigned for FT and a binary string of 5 bits is assigned for FD.
- The target output (0000000001) specifies FT as A-G, [0000000010] specifies FT B-G fault, and (1000000000) specifies FT A-B-C fault, and so on.
- The target output (00001) specifies FD as 20 km, (00010) specifies FD as 50 km, and (10000) specifies FT A-B-C and so on.
- The gradient descent algorithm is used to find out the error between actual output and target outputs in feed forward back propagation neural network (FFBPNN).

Table 4 to *Table 6* displays values of Zap read by phases A, B, and C for FIA = 90^0, 45^0, 30^0, and 0^0 for different FT when a fault is created at 20 km, 100 km, and 160 km respectively with and without R_F of 10 Ω. It is observed that Zap measured by each phase for L-G faults is the same. The same kinds of results are observed for LL, LLG, and LLL faults with different FD, FIA, and R_F.

Table 4 Zap at FIA=90^0, 45^0, 30^0, and 0^0, FD=20 Km

R_F in Ω	Faults	LG fault			LL fault			LLG and LLL fault			
	FT →	**A-G**	**B-G**	**C-G**	**A-B**	**B-C**	**C-A**	**A-B-G**	**B-C-G**	**C-A-G**	**A-B-C**
	Phase ↓	**Z_{ap}** in Ω			**Z_{ap}** in Ω			**Z_{ap}** in Ω			
0	A	0.612	3.73	3.57	3.04	158	3.120	0.58	4.36	0.69	0.79
	B	3.57	0.612	3.73	3.12	3.04	158	0.69	0.58	4.36	0.79
	C	3.73	3.57	0.612	158	3.12	3.04	4.36	0.69	0.58	0.78
10	A	1.593	2.66	4.75	4.36	159.3	1.859	1.485	4.52	1.70	1.6
	B	4.75	1.593	2.66	1.86	4.36	159.3	1.70	1.485	4.52	1.61
	C	2.66	4.75	1.593	159.3	1.86	4.36	4.52	1.70	1.485	1.6

Table 5 Zap at FIA=90^0, 45^0, 30^0, and 0^0, FD=100 Km

R_F in Ω	Faults	LG fault			LL fault			LLG and LLL fault			
	FT →	**A-G**	**B-G**	**C-G**	**A-B**	**B-C**	**C-A**	**A-B-G**	**B-C-G**	**C-A-G**	**A-B-C**
	Phase ↓	**Z_{ap}** in Ω			**Z_{ap}** in Ω			**Z_{ap}** in Ω			
0	A	3.07	8.32	7.69	6.13	175	6.4	3.08	10.43	3.69	3.93
	B	7.69	3.07	8.32	6.4	6.13	175	3.69	3.08	10.43	3.96
	C	8.32	7.69	3.07	175	6.4	6.13	10.43	3.69	3.08	3.9
10	A	3.572	7.15	8.837	7.261	176.2	5.451	3.346	10.41	4.29	4.217
	B	8.837	3.572	7.15	5.45	7.26	176.2	4.29	3.346	10.41	4.26
	C	7.15	8.837	3.572	176.2	5.45	7.26	10.41	4.29	3.346	4.20

Table 6 Zap at FIA=90^0, 45^0, 30^0, and 0^0, FD=160 km

R_F in Ω	Faults	LG fault			LL fault			LLG and LLL fault			
	FT →	**A-G**	**B-G**	**C-G**	**A-B**	**B-C**	**C-A**	**A-B-G**	**B-C-G**	**C-A-G**	**A-B-C**
	Phase ↓	**Z_{ap}** in Ω			**Z_{ap}** in Ω			**Z_{ap}** in Ω			
0	A	4.94	11.8	10.76	8.71	175	9.22	5.04	14.77	6.02	6.33
	B	10.76	4.94	11.8	9.22	8.71	175	6.02	5.04	14.77	6.38
	C	11.8	10.76	4.94	175	9.22	8.71	14.77	6.02	5.04	6.29

10	A	5.346	10.63	11.89	9.758	176.1	8.357	5.183	14.74	6.55	6.537
	B	11.89	5.346	10.63	8.36	9.76	176.1	6.55	5.183	14.74	6.60
	C	10.63	11.89	5.356	176.1	8.36	9.76	14.74	6.55	5.183	6.51

4.1Fault type identification using ANN

ANN FT identifier is trained using three inputs such as Zap_A, Zap_B, and Zap_C, and the outputs are displayed using 10 output nodes, such as F_0-F_9 as shown in *Figure 8*. Error signals are transmitted to backward layers during learning, and weights are modified and amended. Weights are locked to estimate output for the latest inputs once the ANN is trained for a specific set of the training dataset. There are three input nodes in the ANN. The number of hidden neurons is adjusted between 15, 20, 25, and 30. Whereas, the learning rate is tuned for 0.001 and 0.005. During ANN training, the number of epochs is kept at 300. The effectiveness of FFBPNN for different parameters is shown in *Table 7*. It is observed that FFBPNN's highest accuracy of 99.21% is obtained with a learning rate of 0.005 and with 25 hidden layers.

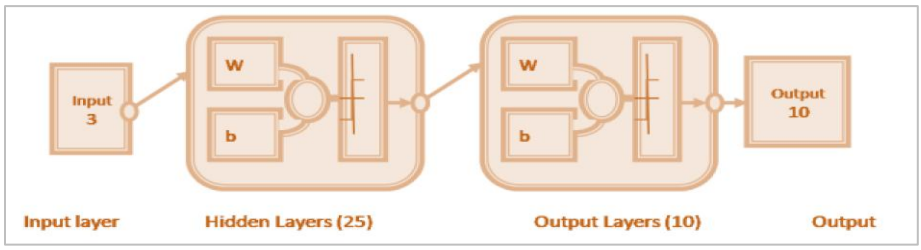

Figure 8 Layer structure (3-25-10) FFBPNN

Table 7 Percentage accuracy for various layer structures of FFBPNN

S. No.	Structure	Learning rate	Accuracy (%)
1	3-15-10	0.005	93.67
2	3-20-10	0.005	97.12
3	**3-25-10**	**0.005**	**99.21**
4	3-30-10	0.005	95.09
5	3-15-10	0.001	95.57
6	3-20-10	0.001	97.45
7	3-25-10	0.001	97.45
8	3-30-10	0.001	96.73

The outputs of types of faults are presented using F_0-F_9 as shown in *Table 8*. A binary string of 9 bits is allocated for identifying ten faults. The desired outcome of ANN with binary bits (0000000001) represents phase A-G fault. Whereas, (0000000010) indicates B-G fault and (1000000000] as A-B-C fault and so on. A total of 400 events were created to generate data required for FT identification.

Table 8 Apparent impedance at different FT, FIA, FD and RF for FT identification

Event No.	Input Parameters				Apparent Impedance, *Zap* (Ω)			Output Bits (Fault type)									
	FT	FIA (deg)	FD (km)	R_F (Ω)	Zap_A	Zap_B	Zap_C	F_9	F_8	F_7	F_6	F_5	F_4	F_3	F_2	F_1	F_0
1	**A-G**	0	20	0	0.612	3.570	3.730	0	0	0	0	0	0	0	0	0	**1**
2	**A-G**	0	50	0	1.530	5.100	5.400	0	0	0	0	0	0	0	0	0	**1**
43	**B-G**	0	100	0	8.32	3.07	7.69	0	0	0	0	0	0	0	0	**1**	0
48	**B-G**	0	100	10	7.152	3.569	8.839	0	0	0	0	0	0	0	0	**1**	0
329	**C-A-G**	0	150	10	6.17	14.05	4.868	0	**1**	0	0	0	0	0	0	0	0
334	**C-A-G**	30	150	0	5.640	14.08	4.710	0	**1**	0	0	0	0	0	0	0	0
385	**A-B-C**	45	160	0	6.330	6.38	6.29	**1**	0	0	0	0	0	0	0	0	0
400	**A-B-C**	90	160	10	6.60	6.59	6.51	**1**	0	0	0	0	0	0	0	0	0

4.2Fault location identification using ANN

ANN Fault locator is trained using three inputs such as Zap_AB, Zap_BC, and Zap_CA as shown in *Figure 9*. Five output nodes such as F_{D0}-F_{D4} are used to show the outputs. *Table 9* shows the effectiveness of FFBPNN for different variables. It is observed that the highest accuracy of 99.01% is obtained with a learning rate of 0.005 and with 20 hidden layers. The outputs/ fault locations are presented using F_{D4} - F_{D0}. A four-bit binary string is assigned to each of the five locations.

The ANN's expected output (00001), (000010), and (01000) indicates faults located at a distance of 20 km, 50 km, and 150 km respectively as shown in *Table 10*. A total of 160 events are created to generate data required for FD identification.

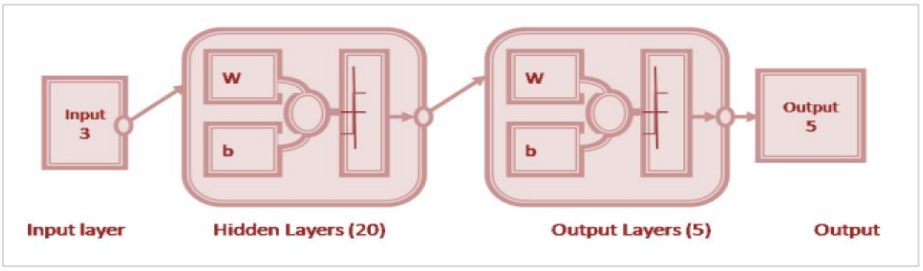

Figure 9 Layer structure (3-20-5) FFBPNN

Table 9 Percentage accuracy for various layer structures of FFBPNN

S. No.	Structure	Learning rate	Accuracy (%)
2	3-15-5	0.005	94.50
3	**3-20-5**	**0.005**	**99.01**
4	3-25-5	0.005	98.33
5	3-30-5	0.005	95.00
8	3-15-5	0.001	95.75
9	3-20-5	0.001	97.00
10	3-25-5	0.001	97.82
11	3-30-5	0.001	96.00

Table 10 Apparent impedance at different FT, FIA, FD, and RF for fault locations

Event	Parameters				Apparent impedance, *Zap* (Ω)			Output bits (Fault Location)				
No	FT	FIA (Deg)	FD (km)	R_F (Ω)	Zap_AB	Zap_BC	Zap_CA	F_{D4}	F_{D3}	F_{D2}	F_{D1}	F_{D0}
1	**A-B**	0	20	0	0.789	9.470	8.50	0	0	0	0	**1**
6	**A-B**	45	20	10	1.590	8.13	9.85	0	0	0	0	**1**
44	**B-C**	30	50	10	11.868	2.43	10.59	0	0	0	**1**	0
45	**B-C**	45	50	0	10.53	1.975	11.920	0	0	0	**1**	0
86	**C-A**	45	100	10	14.959	15.32	4.22	0	0	**1**	0	0
87	**C-A**	90	100	0	16.260	14.00	3.950	0	0	**1**	0	0
154	**A-B-C**	0	160	10	6.53	6.53	6.53	**1**	0	0	0	0
160	**A-B-C**	90	160	10	6.535	6.53	6.53	**1**	0	0	0	0

4.3Model validation

A total of 400 and 160 experimental runs were executed for model validation to identify FT and FD on TL's. *Table 11* shows one run to evaluate the target and actual outputs for FIA set to 0^0, FD of 160 Km, and R_F value equal to 10 Ω. Whereas, *Table 12* displays the target and actual outputs for FIA set to 0^0, FT type B-C and A-B-C as well as R_F value equal to 10 Ω. For model validation, low and high output is designated as 0 and 1. In practice, actual low values of outputs are approximated as 0 and high values of outputs as 1. From the obtained results, it is observed that actual outputs are approximately similar to the target output.

Table 11 Fault type identification with FIA=0^0, FD=160 km and R_F=10Ω

FT	Target Output										Actual Output									
	F_9	F_8	F_7	F_6	F_5	F_4	F_3	F_2	F_1	F_0	F_9	F_8	F_7	F_6	F_5	F_4	F_3	F_2	F_1	F_0
AG	0	0	0	0	0	0	0	0	0	**1**	0.004	0.013	0.02	0.016	0.003	0.005	0.001	0.007	0.008	**0.993**
BG	0	0	0	0	0	0	0	0	**1**	0	0.005	0.018	0.021	0.019	0.003	0.006	0..002	0.013	**0.984**	0.007
CG	0	0	0	0	0	0	0	**1**	0	0	0.013	0.006	0.003	0.001	0.012	0.005	0.003	**0.978**	0.002	0.022
AB	0	0	0	0	0	0	**1**	0	0	0	0.002	0.014	0.007	0.002	0.011	0.004	**0.981**	0.003	0.001	0.006
BC	0	0	0	0	0	**1**	0	0	0	0	0.002	0.004	0.002	0.005	0.017	**0.982**	0.006	0.005	0.001	0.002
CA	0	0	0	0	**1**	0	0	0	0	0	0.001	0.002	0.005	0.018	**0.968**	0.022	0.004	0.003	0.005	0.006
ABG	0	0	0	**1**	0	0	0	0	0	0	0.010	0.011	0.021	**0.992**	0.013	0.001	0.006	0.005	0.002	0.003
BCG	0	0	**1**	0	0	0	0	0	0	0	0.003	0.020	**0.97**	0.019	0.001	0.005	0.002	0.004	0.005	0.004
CAG	0	**1**	0	0	0	0	0	0	0	0	0.004	**0.988**	0.009	0.006	0.003	0.001	0.002	0.008	0.009	0.003
ABC	**1**	0	0	0	0	0	0	0	0	0	**0.991**	0.002	0.015	0.012	0.006	0.004	0.003	0.001	0.002	0.007

Table 12 Fault location identification with FIA=0^0, FT=B-C, A-B-C and R_F as 10 Ω

FT	FD	Target Output					Actual Output				
		F_{D4}	F_{D3}	F_{D2}	F_{D1}	F_{D0}	F_{D4}	F_{D3}	F_{D2}	F_{D1}	F_{D0}
B-C	20	0	0	0	0	**1**	0.005	0.001	0.007	0.008	**0.993**
	50	0	0	0	**1**	0	0.006	0..002	0.013	**0.984**	0.007
	100	0	0	**1**	0	0	0.005	0.003	**0.978**	0.002	0.022
	150	0	**1**	0	0	0	0.004	**0.981**	0.003	0.001	0.006
	160	**1**	0	0	0	0	**0.985**	0.018	0.008	0.002	0.003
A-B-C	20	0	0	0	0	**1**	0.008	0.001	0.004	0.003	**0.991**
	50	0	0	0	**1**	0	0.004	0.002	0.021	**0.994**	0.003
	100	0	0	**1**	0	0	0.016	0.002	**0.988**	0.013	0.017
	150	0	**1**	0	0	0	0.011	**0.984**	0.014	0.005	0.001
	160	**1**	0	0	0	0	**0.996**	0.0016	0.005	0.010	0.022

For FT C-A-G, the target output F_8 should be 1 and for the remaining FT's the target output should be 0. The proposed model can achieve actual output F_8 as 0.988, which is further approximated as 1 in *Table 11*. Similarly, for FD set at 150 km and FT as A-B-C, the target output has 1 value. Whereas, the model is achieving actual output as 0.984≈1 as shown in *Table 12*. It is seen that mean square error (MSE) identified in output is 0.016 and the training time required is 0.0016 sec on a machine at 1 GHz.

- *Table 8* shows the target and actual outputs for eight cases (out of 400 with FIA=0^0, FD=160km, and RF as 10 Ω for FT identification.
- *Table 10* shows the target and actual outputs for another eight cases out of 160 with FIA=0^0, FT=B-C, A-B-C, and RF as 10 Ω for FD identification.

For validation, more data is used to train the model, more effective pattern attributes are identified, and real-valued numeric attributes are rescaled into the range 0 and 1.

5.Discussions

In this paper, the essential step considered in experimentation is to verify that the faithful transformation of current from the primary to the secondary side is achieved with RC. The proposed method for FT and FD identification is evaluated in terms of accuracy by considering various combinations of the input, hidden and output layer. From the result analysis for FT identification, it is seen that for three input, twenty-five hidden, and five output layer structures (3–25–10), FFBPNN with a

learning rate of 0.005, the system is able to achieve an accuracy of 99.33%. The combination of three input, twenty-five hidden, and five output layer structures (3–20–5) FFBPNN with the same learning rate of 0.005, the proposed method, has achieved an accuracy of 99.01% in determining FD location. Further the proposed fault diagnostic approach is also compared with the existing methods. When compared to other approaches, it is observed that the proposed model offers better accuracy for FT and FD identification, as shown in *Table 13*. Highest accuracy is observed in proposed method, due to faithful transformation of current form primary to secondary side as CT is replaced by RC. The steps involved in other method like feature extraction of the distorted current waveform gets completely eliminated. This enhances the speed, reliability and generalisation of the proposed method.

Table 13 Comparative study of fault diagnosis methods

Particulars		Accuracy
Combined Fault Location and Classification for Power Transmission Lines Fault Diagnosis with Integrated Feature Extraction [5]		**98.22 %**
A new FDOST entropy-based intelligent digital relaying for detection, classification, and localization of faults on the hybrid transmission line [42]		**98.2 %**
Probabilistic transmission line fault diagnosis using autonomous neural models, (For fault classification) [43]		**97 %**
Transmission Line Fault analysis using ANN and RC (**Proposed**)	FT identification	**99.21%**
	FD identification	**99.01%**

Advantages and limitations

The main advantage of RC is its ability to be installed without disrupting the circuit through which the current is to be measured. RC also responds well to rapidly changing currents because of its low inductance. However, RC has a lower sensitivity and smaller output voltage since it has no ferromagnetic core. As a result, whenever RC is to be used for current measurement, it needs additional signal processing circuits and an integrator circuit, increasing the coil circuitry. Hence, in DPS, faults nearby the system bus as well as low-magnitude current faults may not be correctly diagnosed using RC.

A complete list of abbreviations is shown in *Appendix I.*

6.Conclusion and future work

ANN-based technique for fault diagnosis on high voltage TL is presented using RC as a current transducer. It uses an estimated value of Zap's for ten types of faults that are created at different locations on a TL transmission line with different R_F's and FIA's. In this paper, PSCAD-EMTDC 4.1 simulation software is used for simulation. The proposed model achieves a measured value of outputs that are same as the targeted outputs. For the experimentation, a total of 160 events are created to generate required test pattern for FD identification. Thereafter 400 events are also created to obtain required test pattern for FT identification. It is seen that TL fault analysis using ANN and RC as the current transducer is able to achieve an accuracy of 99.21 % for fault type identification and 99.01 % for fault location identification.

Hence, it is concluded that the proposed DPS performs accurately for identification of type and location of fault as compared to existing available methods. The accuracy can be further enhanced by fine-tuning of ANN parameters.

It is necessary to find the fault in multi-terminal lines without using the data from each terminal. Further, the measured data is not accessible or contains related errors. As a result, finding faults in multi-terminal lines without having access to all the data is a major problem that necessitates more investigation.

Acknowledgment

None.

Conflicts of interest

The authors have no conflicts of interest to declare.

Author's contribution statement

A. N. Sarwade: Conceptualization and writing– original draft. **M. M. Jadhav:** Data verification and validation-review and editing**. Shivprasad P. Patil:** Analysis and interpretation of results.

References

[1] Grigsby LL. Electric power generation, transmission, and distribution. CRC Press; 2007.

[2] Sanjeevikumar P, Chenniappan S, Holm-nielsen JB, Sivaraman P. Power quality in modern power systems. Academic Press; 2020.

[3] Bamber M, Bergstrom M, Darby A, Darby S, Elliott G. Network protection & automation guide (Protective Relays, Measurement & Control). Alstom Grid; 2011.
[4] Anderson PM, Henville C, Rifaat R, Johnson B, Meliopoulo S. Analysis of distance protection. Wiley-IEEE Press. 2022; 378-417.
[5] Chen YQ, Fink O, Sansavini G. Combined fault location and classification for power transmission lines fault diagnosis with integrated feature extraction. IEEE Transactions on Industrial Electronics. 2017; 65(1):561-9.
[6] Ciufo J, Cooperberg A. Power system protection: fundamentals and applications. John Wiley & Sons; 2021.
[7] Ziegler G. Numerical distance protection: principles and applications. John Wiley & Sons; 2011.
[8] Das JC. Arc flash hazard analysis and mitigation. John Wiley & Sons; 2020: 406-34.
[9] Paithankar YG, Bhide SR. Fundamentals of power system protection. PHI Learning Pvt. Ltd.; 2022.
[10] https://nptel.ac.in/courses/108101039. Accessed 28 January 2023.
[11] Hinge T, Dambhare S. Synchronised/unsynchronised measurements based novel fault location algorithm for transmission line. IET Generation, Transmission & Distribution. 2018; 12(7):1493-500.
[12] Solak K, Herlender J, Iżykowski J. Transmission line impedance-differential protection with improved stabilization for external fault cases. In 19th international scientific conference on electric power engineering 2018 (pp. 1-6). IEEE.
[13] Tajdinian M, Bagheri A, Allahbakhshi M, Seifi AR. Framework for current transformer saturation detection and waveform reconstruction. IET Generation, Transmission & Distribution. 2018; 12(13):3167-76.
[14] Naseri F, Kazemi Z, Arefi MM, Farjah E. Fast discrimination of transformer magnetizing current from internal faults: an extended Kalman filter-based approach. IEEE Transactions on Power Delivery. 2017; 33(1):110-8.
[15] Abdoos AA. Detection of current transformer saturation based on variational mode decomposition analysis. IET Generation, Transmission & Distribution. 2016; 10(11):2658-69.
[16] Alderete L, Tavares MC, Magrin F. Hardware implementation and real time performance evaluation of current transformer saturation detection and compensation algorithms. Electric Power Systems Research. 2021; 196(2021):1-7.
[17] Viawan FA, Wang J, Wang Z, Yang WY. Effect of current sensor technology on distance protection. In IEEE/PES power systems conference and exposition 2009 (pp. 1-7). IEEE.
[18] Kojovic LA. PCB Rogowski coil designs and performances for novel protective relaying. In power engineering society general meeting (IEEE Cat. No. 03CH37491) 2003 (pp. 609-14). IEEE.
[19] Shafiq M, Stewart BG, Hussain GA, Hassan W, Choudhary M, Palo I. Design and applications of Rogowski coil sensors for power system measurements: a review. Measurement. 2022.
[20] Nassisi V. In-depth study of the behavior of the Rogowski coil for fast current pulses. Measurement. 2022.
[21] El-shahat M, Tag EE, Mohamed NA, El-morshedy A, Ibrahim ME. Measurement of power frequency current including low-and high-order harmonics using a Rogowski coil. Sensors. 2022; 22(11):1-15.
[22] Rind YM, Raza MH, Zubair M, Mehmood MQ, Massoud Y. Smart energy meters for smart grids, an internet of things perspective. Energies. 2023; 16(4):1-35.
[23] Dopierała P. Fault detection method for energy measurement systems equipped with a Rogowski coil using the coil's response to a unit voltage jump and a fully convolutional neural network. Measurement. 2022.
[24] Ray P, Panigrahi BK, Senroy N. Extreme learning machine based fault classification in a series compensated transmission line. In international conference on power electronics, drives and energy systems 2012 (pp. 1-6). IEEE.
[25] Watanabe Y, Kato M, Yahagi T, Murayama H, Yamada N, Yoshida K, et al. MEMS Rogowski coil current sensor with spiral return coil. Electrical Engineering in Japan. 2022; 215(4):197-204.
[26] Tan Q, Zhang W, Tan X, Yang L, Ren Y, Hu Y. Design of open-ended structure wideband PCB Rogowski coil based on new winding method. Electronics. 2022; 11(3):1-18.
[27] Zhang T, Shillaber L, Long T. High bandwidth solenoidal PCB Rogowski coil. In PCIM Europe; international exhibition and conference for power electronics, intelligent motion, renewable energy and energy management 2022 (pp. 1-9). VDE.
[28] Han F, Yu X, Al-dabbagh M, Wang Y. Locating phase-to-ground short-circuit faults on radial distribution lines. IEEE Transactions on Industrial Electronics. 2007; 54(3):1581-90.
[29] Malathi V, Marimuthu NS, Baskar S, Ramar K. Application of extreme learning machine for series compensated transmission line protection. Engineering Applications of Artificial Intelligence. 2011; 24(5):880-7.
[30] Megahed AI, Moussa AM, Bayoumy AE. Usage of wavelet transform in the protection of series-compensated transmission lines. IEEE Transactions on Power Delivery. 2006; 21(3):1213-21.
[31] Ferreira VH, Zanghi R, Fortes MZ, Sotelo GG, Silva RD, Souza JC, et al. A survey on intelligent system application to fault diagnosis in electric power system transmission lines. Electric Power Systems Research. 2016; 136:135-53.
[32] Mirzaei M, Vahidi B, Hosseinian SH. Accurate fault location and faulted section determination based on deep learning for a parallel-compensated three-terminal transmission line. IET Generation, Transmission & Distribution. 2019; 13(13):2770-8.

[33] Prasad CD, Nayak PK. A DFT-ED based approach for detection and classification of faults in electric power transmission networks. Ain Shams Engineering Journal. 2019; 10(1):171-8.
[34] Subashini A, Claret SA. A literature survey on fault identification and classification system using machine learning. In AIP conference proceedings 2022. AIP Publishing LLC.
[35] Blackburn JL, Domin TJ. Protective relaying: principles and applications. CRC Press; 2006.
[36] Kojovic LJ. Application of Rogowski coils used for protective relaying purposes. In IEEE PES power systems conference and exposition 2006 (pp. 538-43). IEEE.
[37] Jadhav MM. Machine learning based autonomous fire combat turret. Turkish Journal of Computer and Mathematics Education. 2021; 12(2):2372-81.
[38] Sarwade AN, Katti PK, Ghodekar JG. Use of Rogowski coil as current transducer for distance relay reach correction. International Journal on Electrical Engineering and Informatics. 2016; 8(4):803-19.
[39] https://www.pscad.com/knowledge-base/article/698. Accessed 28 January 2023.
[40] Sarwade AN, Katti PK, Ghodekar JG. Reach and operating time correction of digital distance relay. International Journal of Electrical and Computer Engineering. 2017; 7(1):58-67.
[41] Kojovic LA. Comparative performance characteristics of current transformers and non-conventional current sensors. In CIRED 20th international conference and exhibition on electricity distribution-part 1 2009 (pp. 1-4). IET.
[42] Patel B. A new FDOST entropy based intelligent digital relaying for detection, classification and localization of faults on the hybrid transmission line. Electric Power Systems Research. 2018; 157:39-47.
[43] Ferreira VH, Zanghi R, Fortes MZ, Gomes JS, Da SAP. Probabilistic transmission line fault diagnosis using autonomous neural models. Electric Power Systems Research. 2020; 185:1-10.

Mr. A. N. Sarwade was born in Maharashtra, India in 1977. He received his graduate degree from WCE Sangli, Shivaji University in 1998 and his post-graduate degree from COEP, Pune University in 2006. He received his Ph.D. from Dr. BATU University, Lonere in 2018. He is presently working as a Professor in Sinhgad College of Engineering, Pune. His research interest includes Power System Protection and Electric Machines.
Email: asarwade@yahoo.com

M. M. Jadhav has completed his Ph.D. in Electronics and Telecommunication in 2018 from the Government College of Engineering, Pune. He is presently working as Head and Professor in the E&Tc Department, NBN Sinhgad Technical Institutes Campus, Pune. His Area of interest lies in Network Coding, Wireless Communication, and Optimisation Techniques.
Email: makj123@yahoo.com

Shivprasad P. Patil has completed his Ph.D. in 2018 from AU, Denmark. He is presently working as Principal/ Director, NBN Sinhgad Technical Institutes Campus, Pune. His Area of interest lies in Video Processing, the Internet of Things and Optimisation Techniques.
Email: sppatil1212@gmail.com

Appendix I

S. No.	Abbreviation	Description
1	ANN	Artificial Neural network
2	AB	Phase A to Phase B
3	ABC	Phase A to Phase B to Phase C
4	ABG	Phase A to Phase B to Ground
5	AG	Phase A to Ground
6	BC	Phase B to Phase C
7	BCG	Phase B to Phase C to Ground
8	BG	Phase B to Ground
9	CA	Phase C to Phase A
10	CG	Phase C to Ground
11	CAG	Phase C to Phase A to Ground
12	CT	Current Transformer
13	DPS	Distance Protection Scheme
14	DP	Distance Protection
15	DR	Distance Relay
16	EMTDC	Electromagnetic Transient Dc
17	FT	Fault Type
18	FFBPNN	Feed Forward Back Neural Network
19	FD	Fault Distance/ Location
20	FIA	Fault Inception Angle
21	HV	High Voltage
22	I_A, I_B, I_C	Phase Currents
23	LG	Line to Ground
24	LLG	Line to Line to Ground
25	LLL	Line to Line to Line
26	M	Mutual Inductance
27	MSE	Mean Square Error
28	MVA	Mega Volt Amps
29	n	Turns Density
30	NN	Neural Network
31	PSCAD	Power System Computer Aided Design
32	R_F	Fault Resistance
33	RC	Rogowski Coil
34	TL	Transmission Line
35	Zap	Apparent Impedance
36	VT	Voltage Transformer
37	V_A, V_B, V_C	Phase Voltages
38	WT	Wavelet transform
39	Z_0	Zero Sequence Impedance
40	Z_1	Positive sequence Impedance
41	Z_A, Z_B, Z_C	Line Impedance
42	Z_{AB}, Z_{BC}, Z_{CA}	Line to Line Impedance